THE ASTROPHYSICAL JOURNAL, 372:215–224, 1991 May 1

CENTRAL STAR TEMPERATURES OF LOW-EXCITATION PLANETARY NEBULAE

JAMES B. KALER
Department of Astronomy, University of Illinois, 103 Astronomy Bldg., 1002 West Green St. Urbana, IL 61801

AND

GEORGE H. JACOBY
Kitt Peak National Observatory, National Optical Astronomy Observatories,[1] P.O. Box 26732, Tucson, AZ 85726
Received 1990 August 6; accepted 1990 October 18

ABSTRACT

We correlate Kaler's Stoy (energy balance) and new Zanstra temperatures of the central stars of low-excitation planetary nebulae with the intensity of [O III] λ5007, where all objects are small (young) and have no or weak He II λ4686 (intensity < 10). More recent energy balance temperatures are shown to be unsatisfactory for this class of objects. We find $T_S = 25{,}840 + 19.30I(\lambda5007) + 2.8229 \times 10^{-2}\ I^2(\lambda5007) - 1.46115 \times 10^{-5}I^3(\lambda5007)$, $T_Z(\mathrm{H}) = 30{,}370 + 14.26I(\lambda5007)$, and $T_Z = 28{,}380 + 26.13I(\lambda5007)$, where for the last we substitute T_Z(He II) for T_Z(H) in cases where He II is detected. Comparisons among the temperatures show that planetaries may start becoming optically thin for central star temperatures in the 40,000 K–50,000 K range and that the Zanstra discrepancy for this class of objects may be resolved by invoking low optical depth; an excess in the stellar He^+ Lyman continuum may also provide a contribution. The Stoy calibration seems to give the best estimate of central star temperatures from the λ5007 line. The correlations are valuable for determining effective temperatures in cases where no nuclei can be detected and are especially useful for extragalactic objects.

Subject headings: nebulae: planetary — stars: early-type

1. INTRODUCTION

Without question, the most important single parameter for a planetary nebula nucleus is its effective temperature. A variety of methods are available for its determination, including the classic Zanstra procedure (Zanstra 1927; Harman & Seaton 1964), the Stoy or energy-balance method (Stoy 1933; Kaler 1976a), measurement of ultraviolet energy distributions (Pottasch et al. 1978), the modeling of stellar absorption lines (Méndez, Kudritzki, & Simon 1985), modeling of nebular ionic distributions (Natta, Pottasch, & Preite-Martinez 1980), and the "crossover" technique, which uses the He II λ4686 fluxes of optically thick nebulae (Ambartsumyan 1932; Kaler & Jacoby 1989). The subject is reviewed more fully by Kaler (1989).

The Zanstra method requires high-quality central star magnitudes, the absorption line procedure needs optical spectra with very high signal-to-noise ratios, and direct observations in the ultraviolet are compromised by the lack of sensitivity of the flux distribution to temperature. Good spectra can be acquired only for quite-bright nuclei or for those stars that are well-separable from their nebulae (such as for large, old objects), and ultraviolet data are again restricted to brighter stars in addition to those with relatively low interstellar extinctions.

Magnitudes are available for large numbers of objects. For large nebulae with well-isolated stars their measurement provides little difficulty. However, for angularly compact objects, especially for those with faint central stars, the nebular continuum can be quite difficult to separate from the stellar. If the star is reasonably bright they can be effectively distinguished spectroscopically, where we calculate the expected nebular continuum on the basis of the Hβ flux, the He^+ and He^{+2} abundances, and the electron temperature and density. Kohoutek & Martin (1981a) and Shaw & Kaler (1985) used narrow-band interference filters to so extract stellar magnitudes, and others (de Freitas-Pacheco, Codina, & Viadana 1986; Tylenda et al. 1990, for example) employed conventional spectroscopy. However, this method also presents its difficulties, chief of which are the appropriate electron temperatures to apply to the nebular continua and the difficulty of estimating the two-quantum continua for dense objects. An even more effective technique involves subtractive imaging (Jacoby 1988; Heap & Hintzen 1990; Jacoby & Kaler 1989), but data derived from it are yet quite limited.

Neither will work well (or at all) if the star is extremely faint. For these nebulae central star temperatures must be determined by procedures that do not directly depend upon central star observations, such as the Stoy (energy balance) and crossover (Kaler & Jacoby 1989) methods (and the various techniques of nebular modeling mentioned above). Yet even these approaches have their limitations: the Stoy and nebular modeling methods require extensive nebular spectroscopy, the Stoy temperatures become problematic for high-excitation objects (Kaler 1976a; Kaler & Jacoby 1990), and the crossover method cannot be used if the nebula is optically thin or if λ4686 is not present.

In order to alleviate some of these problems, Kaler (1978a) simply calibrated the Stoy method with the strength of [O III] λ5007, which rises dramatically as the central star temperature is increased from the minimum of about 25,000 K to the point of the onset of substantial nebular He II near 60,000 K. The correlation thus allows the estimation of central star temperatures in young lower excitation objects even if they are extragalactic. We expand upon this theme in this paper, wherein we provide an improved correlation between λ5007 strengths and the Stoy temperatures in addition to a similar calibration of well-determined Zanstra temperatures. The

[1] The National Optical Astronomy Observatories are operated by the Association of Universities for Research in Astronomy, Inc., under cooperative agreement with the National Science Foundation.

TABLE 1

CENTRAL STAR TEMPERATURES

Nebula (1)	B (2)	V (3)	$-F(\mathrm{H}\beta)$ (4)	I (4686) (5)	c (6)	T_S (7)	T_Z (H) (8)	T_Z[a] (He II) (9)	T_M (10)	I (5007) (11)	R[b] (12)
NGC 40	10.82	10.65	10.66	...	0.76	32	26	...	...	32	
NGC 5315	14.28	14.20	10.42	7.0	0.60	56	65	82	...	778	
NGC 5882	13.48	13.42	10.38	4.0	0.38	61	53	71	...	986	*
NGC 6210	13.00	12.87	10.09	2.4	0.02	58	56	68	...	1046	
NGC 6369	17.00	15.89	11.32	3.7	1.86	65	64	76	75[c]	1302	
NGC 6543	10.87	11.31	9.61	...	0.12	45	47	...	...	656	*
NGC 6567	14.45	14.38	10.95	1.9	0.75	56	47	63	75[c]	889	
NGC 6572	12.75	12.86	9.82	...	0.34	60	66	...	...	1114	
NGC 6578	16.01	15.74	11.57	(1.60)	1.51	...	46	(62)	50[c]	786	*
NGC 6629	13.21	12.97	10.93	...	0.90	45	35	...	50[c]	649	*
NGC 6790	16.30	15.50	10.90	(1.40)	0.83	66	76	(71)	...	1426	*
NGC 6803	16.00	15.20	11.18	3.60	0.79	62	56	72	...	994	*
NGC 6826	10.22	10.69	9.96	...	0.03	47	33	...	...	723	*
NGC 6833	14.95	15.10	11.26	(2.00)	0.19	49	45	(62)	63[c]	726	*
NGC 6891	12.22	12.63	10.66	...	0.23	49	35	...	50[d]	780	*
IC 418	10.00	10.09	9.57	...	0.31	32	38	...	36	144	*
IC 2149	11.28	11.47	10.55	...	0.25	36	30	...	...	485	*
IC 2501	14.41	14.30	10.67	(0.20)	0.53	51	56	(54)	...	824	*
IC 3568	12.47	12.31	10.82	1.20	0.19	61	31	52	50[e]	1070	
IC 4593	10.97	11.17	10.59	...	0.05	43	28	...	...	560	*
IC 4634	13.78	11.98	10.88	...	0.55	55	43	...	...	940	*
IC 4637	12.99	12.47	11.23	...	1.12	...	28	...	47	840	*
IC 4732	...	...	...	1.0	0.28	64	...	[66]	63[c]	1402	
IC 4776	14.19	14.47	10.73	...	1.00	...	53	...	...	841	*
IC 4846	15.28	15.45	11.34	0.60	0.50	61	47	56	...	1178	*
IC 4997	...	...	...	...	1.07	49	...	...	...	582	
IC 5117	17.50	16.70	11.37	8.2	1.31	77	76	90	...	1419	
IC 5217	15.40	15.50	11.17	6.8	0.34	68	53	76	...	1244	*
BD +30	10.06	9.95	10.03	...	0.46	27	30	...	...	7	*
CN 1−5	16.40	16.60	11.25	...	0.41	...	69	...	...	780	
Cn 3−1	...	12.6	10.94	...	0.42	25	31	...	...	17	*
Ha 1−35	15.70	15.30	11.52	...	1.24	...	43	...	...	504	
Ha 1−54	15.70	15.4	11.89	3.0	0.82	...	35	...	...	385	*
Ha 2−1	13.68	13.27	11.45	...	0.91	...	29	...	33	63	*
HB −12	15.20	14.10	11.02	...	1.43	38	48	...	...	407	
He 2−5	14.87	15.47	11.38	(1.4)	0.29	...	44	(59)	...	611	*
He 2−9	17.73	16.53	12.23	...	2.08	...	42	...	...	630	*
He 2−11	...	18.92	12.14	...	2.24	...	89	...	...	1265	
He 2−25	17.08	16.96	12.58	...	2.95	...	29	...	...	488	
He 2−90	16.10	15.88	11.45	(2.0)	1.54	...	51	(66)	...	158	
He 2−97	15.43	15.48	11.44	0.7	0.66	...	45	56	...	712	*
He 2−105	14.99	15.17	11.55	3.3	0.42	...	38	61	...	418	*
He 2−107	16.35	15.51	12.26	(4.)	1.70	...	32	(59)	...	115	
He 2−108	12.77	12.73	11.43	...	0.55	29	26	...	33	197	*
He 2−115	17.37	15.87	12.41	...	2.26	...	34	...	...	587	
He 2−118	16.0	16.1	11.70	...	0.07	...	44	...	...	1211	
He 2−123	17.55	16.84	12.03	...	1.65	...	48	...	...	173	
He 2−131	10.92	10.92	10.16	...	0.19	26	33	...	...	9	
He 2−138	10.76	10.91	10.72	...	0.40	22	26	...	27	4	*
He 2−140	18.40	17.20	12.48	...	1.91	...	42	...	...	38	
He 2−142[f]	15.88	15.15	11.83	(7.4)	1.55	...	36	(65)	..	0	
He 2−149	17.10	16.10	12.58	...	1.16	...	31	...	...	813	
He 2−155	16.69	16.26	11.64	5.4	1.01	...	51	73	...	1075	
He 2−156	14.55	13.29	12.38	...	1.85	...	22	...	...	26	*
He 2−182	13.35	13.33	10.96	...	0.25	...	36	...	36	290	*
He 2−185	15.97	16.46	11.52	...	0.17	...	52	...	...	1177	
Hu 2−1	13.45	13.35	10.80	...	0.51	36	40	...	...	405	*
J320	14.25	14.38	11.39	3.3	0.30	57	36	59	...	1144	*
M1−11	14.77	14.01	11.83	...	1.62	...	29	...	...	14	*
M1−14	14.37	14.09	11.61	...	0.84	35	31	...	...	276	*
M1−20	17.58	17.1	11.93	...	1.17	...	53	...	...	1015	
M1−26	13.47	12.75	11.12	...	1.70	...	32	...	33	90	*
M1−27	15.60	14.53	12.23	(4.)	2.13	...	28	(55)	...	2	
M1−74	18.80	18.10	11.75	0.4	1.06	...	...	[58]	...	1060	
M2−9	16.29	15.65	11.66	...	1.34	...	44	...	...	102	*
M2−13	19.40	18.80	12.29	...	0.93	...	69	...	...	802	
M2−23	16.60	16.70	11.58	...	0.60	44	56	...	50[c]	947	
M3−1	15.30	15.59	11.32	2	0.24	...	48	65	...	726	*
M3−21	16.20	15.34	11.42	7.5	0.83	...	49	74	...	1520	
Me 1−1	...	...	...	...	0.76	65	...	...	...	1015	
Me 2−2	15.42	16.08	11.16	...	0.23	46	59	...	58[c]	702	
PB−8	13.76	13.80	11.41	3	0.43	...	32	56	...	364	

TABLE 1—*Continued*

Nebula (1)	B (2)	V (3)	$-F(\mathrm{H}\beta)$ (4)	I (4686) (5)	c (6)	T_S (7)	T_Z (H) (8)	T_Z[a] (He II) (9)	T_M (10)	I (5007) (11)	R[b] (12)
PC−11	13.00	12.67	11.45	...	0.89	...	26	...	...	1111	
PC−12	15.39	15.26	11.91	...	0.70	...	33	...	...	315	*
PC−14	17.22	16.51	11.74	9.0	0.66	...	54	79	...	1291	
Pe 1−7[g]	18.30	17.10	12.53	...	2.56	...	40	...	...	0	*
Ps − 1	...	...	...	...	0.20	27	...	...	...	234	
Sn − 1	14.47	14.71	11.73	...	0.17	...	32	...	...	1099	*
Tc−1	11.42	11.59	10.73	...	0.28	...	28	...	33	71	*
Vy 1−1	14.11	14.45	11.53	...	0.07	52	33	56	...	855	*
Vy 2−2	15.91	15.28	11.56	1.5	1.80	56	41	59	...	733	

[a] Parentheses indicate that $I(\lambda4686)$ and T_Z(He II) are very uncertain and that He II λ4686 may be a false detection; brackets around T_Z(He II) indicate that it is a crossover temperature.
[b] Asterisk(*) indicates that the error in both B and V is less than 0.25 magnitudes.
[c] From Aller & Keyes 1987; others in this column from Méndez et al 1988.
[d] Aller & Keyes 1987 and Méndez et al 1988 give the same value.
[e] From Harrington & Feibelman 1983.
[f] Odd, very low λ5007 intensity.
[g] High-density object (unpublished CTIO data).

work also gives us the opportunity to compare the Stoy and Zanstra temperatures so that we might test the Stoy method and examine problems associated with the optical depths of low-excitation objects.

2. THE TEMPERATURES

The calibrating nebulae are listed in Table 1. The first column gives the name, starting with the NGC and IC objects, and then proceeds alphabetically by catlog name. The next five columns give the data required for the calculation of the Zanstra temperatures. The B and V magnitudes in columns (2) and (3) were compiled by averaging the measurements made by de Freitas-Pacheco, Codina, & Viadana (1986), Gathier & Pottasch (1988), Kohoutek & Martin (1981a), Martin (1981), Shaw & Kaler (1985, 1989), Tylenda et al. (1990), and Walton et al. (1986). We discarded any measurements that deviate significantly from the mean. The work of Tylenda et al. (1990) indicates that Shaw & Kaler (1989) measured their most difficult (usually faintest) stars as too bright. Consequently, for those objects for which no measurements other than these two are available, we preferentially select those of Tylenda et al. (1990) if theirs provide the fainter magnitudes. In all cases we averaged the individual magnitudes, not the continuum fluxes. If the measurements are close the difference is slight, and if the scatter is large, the difference is lost in the error. Averaging the magnitudes also weights the mean toward higher numbers (fainter stars), which is actually preferable given the common tendency to measure magnitudes as too bright. The Martin (1981) results were converted to V with the known reddening constant and the assumption of a blackbody flux distribution (see Shaw & Kaler 1989).

The Hβ fluxes, the relative He II (λ4686) intensities [on the usual scale of $I(\mathrm{H}\beta) = 100$], and the reddening constants (c, the logarithmic extinctions at Hβ), presented in the fourth, fifth, and sixth columns, were taken from a compilation by Cahn, Kaler & Stanghellini (1990). In the few instances where the He II fluxes are not global, they were averaged from all available small-aperture photometry. Only those nebulae at the upper end of the temperature range considered exhibit the He II lines. We cut these off at $I(\lambda4686) = 10$; beyond that the [O III] intensities begin to be insensitive to temperature, and in any case the Stoy temperatures are not available. Because the He II lines are weak, they are often unreliable; frequently it is not possible to tell whether they are nebular or stellar in origin. (The low-excitation objects NGC 40 and IC 418 are excellent cases in point: lower resolution observations show a line at λ4686 that was long—and sometimes still is—reported as nebular whereas it is in fact stellar). We list all the available λ4686 intensities, but place those that we believe are unreliable, or are reported as such, in parentheses.

The Stoy temperatures, T_S, are taken from Kaler (1976a, 1978a), and are placed in column (7) of Table 1. We drop M1−58, M1−59, M1−64, and M1−73 as unreliable. We computed the hydrogen and He II Zanstra temperatures, T_Z(H) and T_Z(He II), respectively, from the code described by Kaler (1983b), and give them in columns (8) and (9). Values of T_Z(He II) based on the unreliable He II line intensities are again enclosed in parentheses. For purposes of comparison, we also include the central star temperatures derived from absorption line profile fits by Méndez et al. (1988) and from nebular model analyses by Aller & Keyes (1987) and Harrington & Feibelman (1983), which we call T_M, in column (10). We consider the Méndez et al. (1988) temperatures (which carry no footnotes with the exception of footnote d) as true measurements; the nebular model results are sensitive to other model parameters and are regarded here only as estimates. The relative [O III] (λ5007) intensities, corrected for interstellar extinction, are in column (11). They are all global (or nearly so) and are taken (and averaged) from Acker et al. (1989), Aller & Czyzak (1976), Barker (1978), Capriotti & Daub (1960), Collins, Daub & O'Dell (1961), Kaler (1976b, 1978b, 1980, 1983a), Kohoutek & Martin (1981b), O'Dell (1962, 1963), Torres-Peimbert & Peimbert (1978), and Webster (1976, 1983).

The errors in the Hβ fluxes are all very small, usually no more than 0.01, and the extinctions are generally quite accurate as well. The errors in the hydrogen Zanstra temperatures are dominated by errors in magnitudes that are often quite difficult to measure. Since this is a statistical study, the errors for individual stars are not terribly relevant except to separate really reliable objects from those that are not. Consequently in the last column we place an asterisk if the errors in *both* B and V are less than or equal to 0.25 magnitudes as determined either from a comparison of two or more determinations or from the authors' statements. The errors in T_Z(He II) are further compounded by errors in $I(\lambda 4686)$, which are unknown: it is still quite possible for "reliable" values to be spurious.

3. THE CORRELATIONS

3.1. *Our Stoy Temperatures*

We plot T_S against $I(\lambda 5007)$ in Figure 1, where we see an excellent correlation similar to the one displayed by Kaler (1978a). Such a correlation is expected since the cooling mechanism in planetaries is dominated by the [O III] lines whose intensities are generally the most prominent of the cooling terms in the calculations. A linear fit, shown by the solid line, gives

$$T_S = 25410 + 32.13I \,, \tag{1}$$

where I is the relative intensity in $\lambda 5007$ and we reject the most deviant point, that derived for M2−23. The rms error is 3530 K. In the fits to $I(\lambda 5007)$, here and below, we use the classic least-squares technique in which the variable on the x-axis is assumed to be error-free. The errors in the $\lambda 5007$ intensities are low as the line is so strong, certainly lower relatively than those of the temperatures, so that this procedure is quite appropriate. A cubic fit,

$$T_S = 25{,}840 + 19.30I + 2.8229 \times 10^{-2}I^2 - 1.46115 \times 10^{-5}I^3 \,, \tag{2}$$

also excluding M2−23, does a somewhat better job, resulting in a lower rms error of 3360 K. The results from equations (1), (2), and the quadratic fit given by Kaler (1978a), are all within about 2000 K of one another. We obviously recommend equation (2).

The Zanstra temperatures present an interesting problem. Ordinarily when both H and He II temperatures are available the latter is greater than or equal to the former. The difference is known as the "Zanstra discrepancy." There are two traditional explanations for it that have been argued over for 60 yr: either the star is producing an ultraviolet excess that raises the He II temperature above the effective temperature (favored by Zanstra himself) or the nebula is optically thin in the hydrogen Lyman continuum and thick in the He^+ Lyman continuum, in which case the He II temperature is the one to use (see Harman & Seaton 1964). The matter is discussed further by Kaler (1989). Méndez et al. (1988) produce data supporting the He^+ Lyman excess, whereas the studies of Kaler & Jacoby (1989) and Jacoby & Kaler (1989) find no evidence for an He^+ excess for their high-excitation clearly optically thick objects. It may well be that different explanations are valid for different types of nebulae and different temperature ranges. We will take up the subject again in the next section. But for now we have the question of which values in Table 1 to use. We also have the problem of whether we should use all the data or only those that we designate as most reliable by the asterisk in the last column of the table. We consequently look at correlations done in a variety of ways.

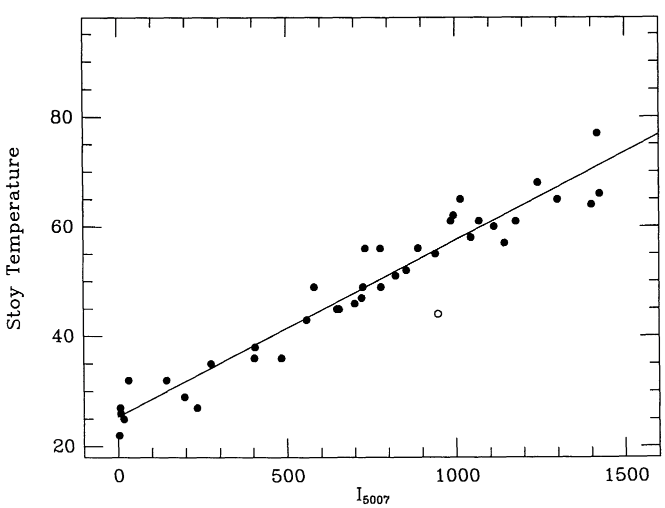

FIG. 1.—The Stoy temperature, T_S, plotted against the intensity of [O III] $\lambda 5007$, $I(\lambda 5007)$. The temperatures are in thousands of kelvins (used for the other figures as well), the solid line is the least-squares fit calculated by assuming that $I(\lambda 5007)$ is error free, and the open symbol is a rejected point (which apply to Figs. 2–6 as well).

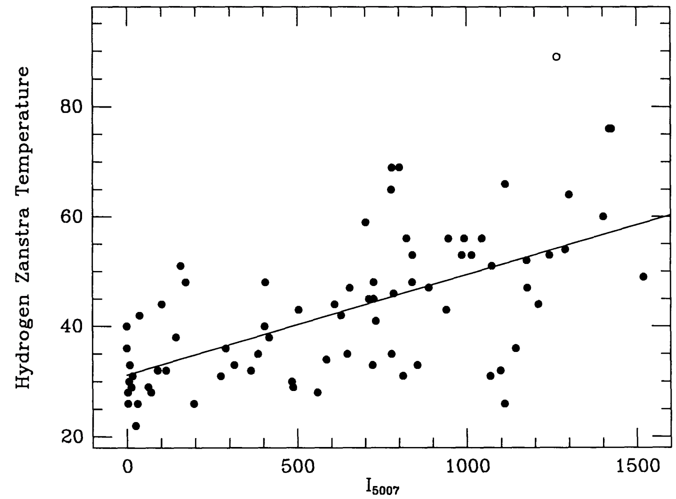

FIG. 2.—The full set of hydrogen Zanstra temperatures, $T_Z(H)$, plotted against $I(\lambda 5007)$, along with a least-squares fit. See Fig. 1.

In Figure 2 we use all the data and plot only the $T_Z(H)$ against $I(\lambda 5007)$. The scatter is such that we need only consider a linear correlation, and find (deleting the anomalous He 2−11)

$$T_Z(H) = 31{,}220 + 18.22I \,. \tag{3}$$

The rms error is now a considerably higher 9890 K. The correlation for only the best (asterisked) stars is then displayed in Figure 3, yielding the relation (less NGC 6790)

$$T_Z(H) = 30{,}370 + 14.26I \,. \tag{4}$$

The scatter is less and we consider this correlation to be superior, supported by a notably lower rms error of 6790 K.

Next, note that as usual the Zanstra discrepancy is quite apparent, as T_Z(He II) is greater than or equal to $T_Z(H)$. For now we assume (and look at the problem more fully in § 4) that the nebulae become optically thin in the hydrogen Lyman continuum at or near the onset of He^+ ionization, which renders the He II lines visible (see Harman & Seaton 1964). Since the hydrogen Lyman continuum photons escape, $T_Z(H)$ will be a lower limit. But the nebulae are still optically thick in the He^+ Lyman continuum, and consequently we substitute the T_Z(He II) for $T_Z(H)$ when they are available. We use only those that we deem reliable (not enclosed in parentheses in Table 1) and plot the full combined set (now called T_Z) with all the data in Figure 4, for which we find (deleting NGC 5315 and PC−11)

$$T_Z = 29{,}700 + 28.84I \,; \tag{5}$$

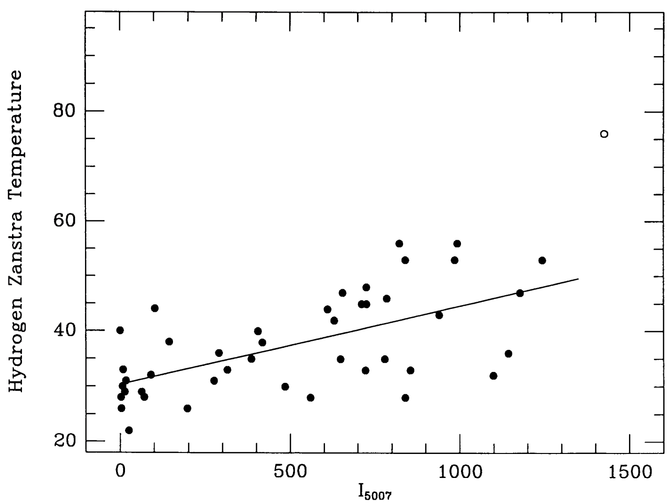

FIG. 3.—The restricted (best data) set of T_Z(H) plotted against $I(\lambda5007)$, along with the least-squares fit. See Fig. 1.

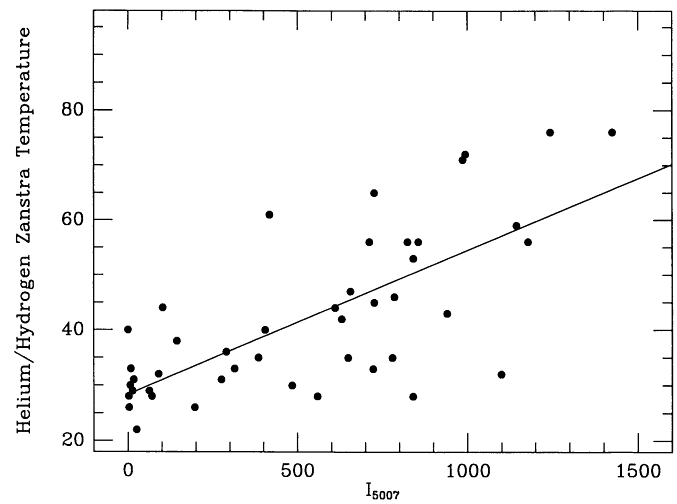

FIG. 5.—The restricted (best data) set of T_Z plotted against $I(\lambda5007)$, along with the least-squares fit. See Fig. 1.

With the restricted set (asterisked stars only) we plot Figure 5 and find (deleting none)

$$T_Z = 28{,}380 + 26.13I\ . \tag{6}$$

Because we combine somewhat disjoint sets, the rms errors jump to 10,920 K and 10,120 K, respectively. Finally, we graph the Méndez et al. (1988) temperatures, T_M, against $I(\lambda5007)$ in Figure 6, for which we obtain

$$T_M = 30{,}270 + 22.42I \tag{7}$$

and a low rms error of 1940 K. This error is so low that errors in the $\lambda5007$ intensities may be significant relative to those in the temperatures, thus producing a problem with the straightforward least-squares procedure. We therefore follow the recommendations of Isobe et al. (1990) and fit relations to *both* the ordinate and abscissa (assuming first one and then the other to be error-free) and adopt the bisector. The result, which differs only slightly, is

$$T_M = 30{,}000 \pm 930 + 23.38 \pm 2.46I \tag{8}$$

(plotted in Fig. 6), with an rms error of 2080 K.

Although it is perhaps redundant, it is highly instructive to compare the various temperatures against one another. However, here we again encounter the same difficulty in the least-squares procedure, since the errors in the ordinate and abscissa are at least roughly comparable to one another. Furthermore, the errors are not easily calculable, nor is all the scatter due to measurement error. In the following we again adopt the bisector to the two least-squares fits as per Isobe et al. (1990). The results are as follows, where we plot: the complete set of T_S against T_Z(H) in Figure 7 to find (less IC 3568)

$$T_S = 3980 \pm 3850 + 0.977 \pm 0.080T_Z(\mathrm{H}) \tag{9}$$

(rms error of 9350 K); the restricted set of T_S against T_Z(H) in

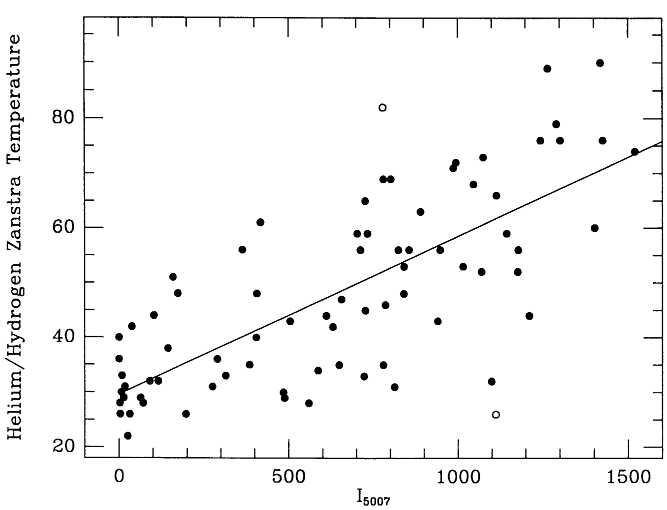

FIG. 4.—The full set of combined hydrogen and He II Zanstra temperatures, T_Z, plotted against $I(\lambda5007)$. The T_Z(He II) substitute for T_Z(H) when reliable He II lines are present. The solid line is again the least-squares fit. See Fig. 1.

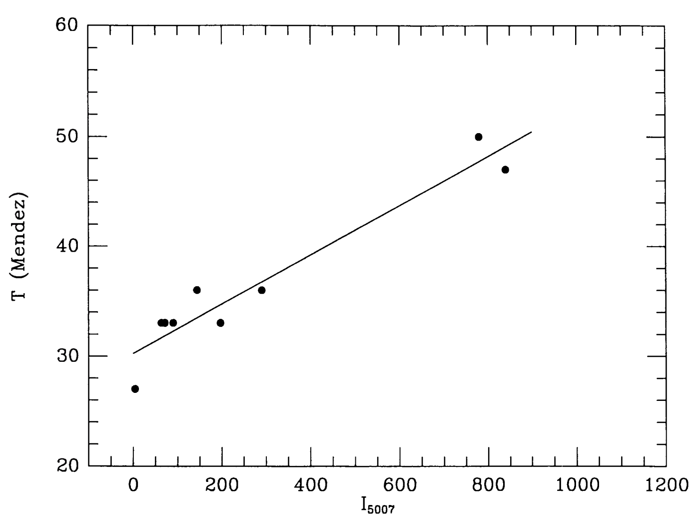

FIG. 6.—T_M, temperatures derived from stellar absorption line profiles, plotted against $I(\lambda5007)$, with a least-squares fit that is the bisector of the individual fits found by assuming first the ordinate and then the abscissa to be error-free.

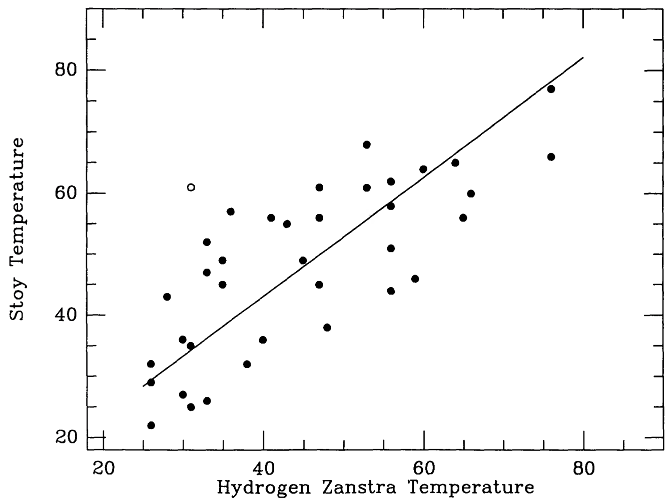

FIG. 7.—The Stoy temperatures, T_S, plotted against the full set of hydrogen Zanstra temperatures, T_Z(H), with a least-squares fit of the type found for Fig. 6. The open symbol represents a rejected point.

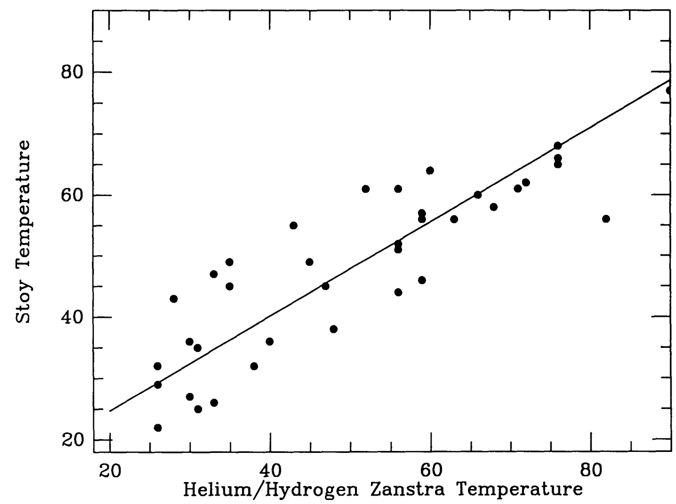

FIG 9.—T_S plotted against the full set of combined hydrogen-He II Zanstra temperatures T_Z, with the least-squares fit of the type found for Fig. 6.

Figure 8, from which (less NGC 6790)

$$T_S = -8970 \pm 5860 + 1.378 \pm 0.149 T_Z(\mathrm{H}) \tag{10}$$

(rms error of 9430 K); the full set of T_S against T_Z (the combined hydrogen and helium Zanstra temperatures) in Figure 9, from which

$$T_S = 9320 \pm 3080 + 0.771 \pm 0.053 T_Z \tag{11}$$

(rms error of 7180 K); the restricted set of T_Z against T_S in Figure 10, from which

$$T_S = 7380 \pm 3770 + 0.841 \pm 0.071 T_Z \tag{12}$$

(rms error of 7090 K); T_S and T_Z(H) against T_Z(He II) in Figure 11 (full sets only); and finally T_S and T_Z(H) against T_M (from absorption line profiles only) in Figure 12.

3.2. *New Stoy Temperatures*

Preite-Martinez et al (1989, 1990) have recently calculated a very large number of Stoy, or energy balance, temperatures

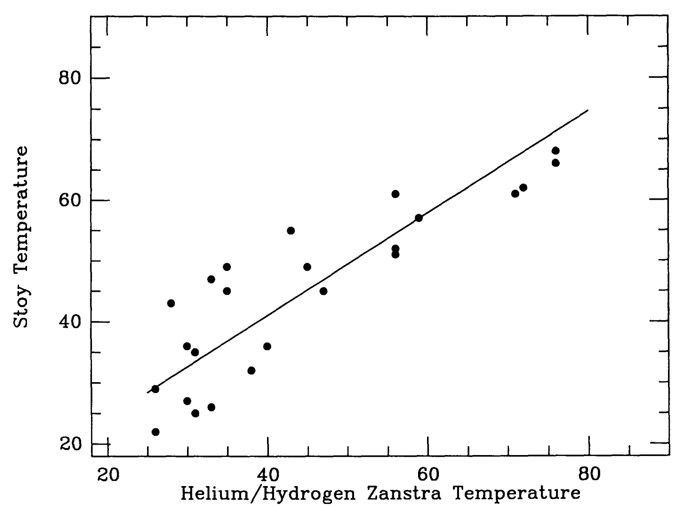

FIG. 10.—T_S plotted against the restricted set of T_Z together with the least-squares fit of the type found for Fig. 6.

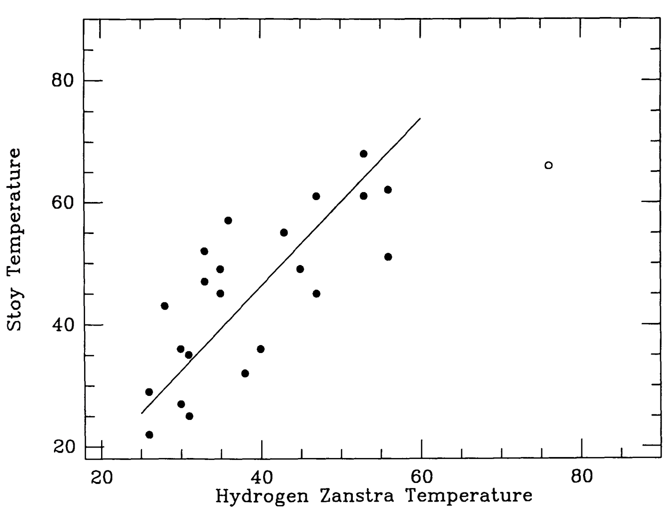

FIG. 8.—T_S plotted against the restricted set of T_Z(H) with a least-squares fit of the type found for Fig. 6. The open symbol represents a rejected point.

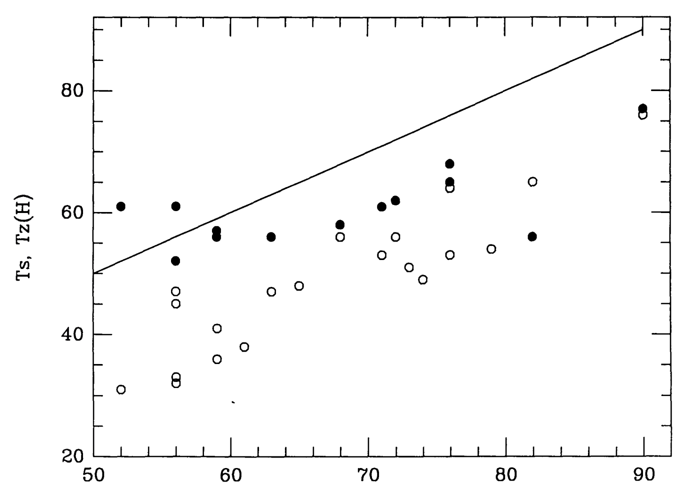

FIG. 11.—T_S (*filled circles*) and T_Z(H) (*open circles*) plotted against T_Z(He II) along with the line of perfect agreement.

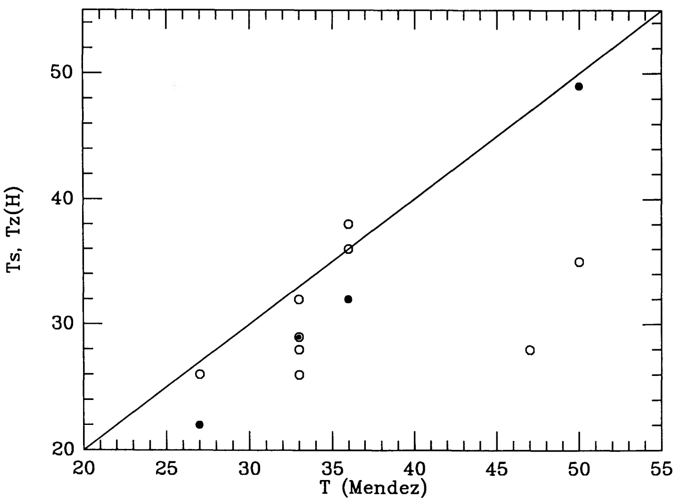

FIG. 12.—T_Z(H) (*open circles*) and T_S (*filled circles*) plotted against the temperatures derived from absorption line profiles, T_M.

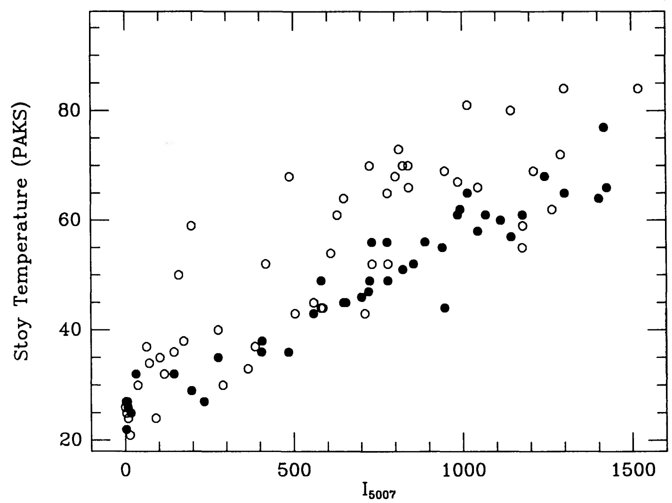

FIG. 14.—T_{PAKS} (*open symbols*) plotted against $I(\lambda 5007)$ from Table 1. The points in Fig. 1 (T_S) are overplotted as filled symbols.

from a new extensive survey of planetary spectra. We test these to see if they are useful for this study. A plot of their Stoy temperatures (T_{PAKS}) against the T_S in Table 1 (Fig. 13) shows a rough correlation with considerable scatter. The agreement is best at low temperatures, but at higher values theirs tend to fall well above ours with theirs on the average 9000 K greater. It rather appears that the line of perfect agreement forms a lower envelope to the distribution. A plot of T_{PAKS} against $I(\lambda 5007)$ in Figure 14 also shows a correlation, as would be expected, but with much greater scatter than seen in Figure 1 (overplotted in Fig. 14). That appears a bit suspicious, but it is possible that Kaler (1976a, 1978a) simply placed much more emphasis on the cooling from the [O III] lines.

The real test is in comparisons with independently determined values, namely the Zanstra temperatures. We show T_{PAKS} plotted against T_Z(H) and T_Z in Figures 15 and 16. They are not much more than scatter diagrams in which the line of perfect agreement appears again to be something of a crude lower limit. T_{PAKS} is plotted against T_M in Figure 16 as well. The distribution displays something of the same effect, although

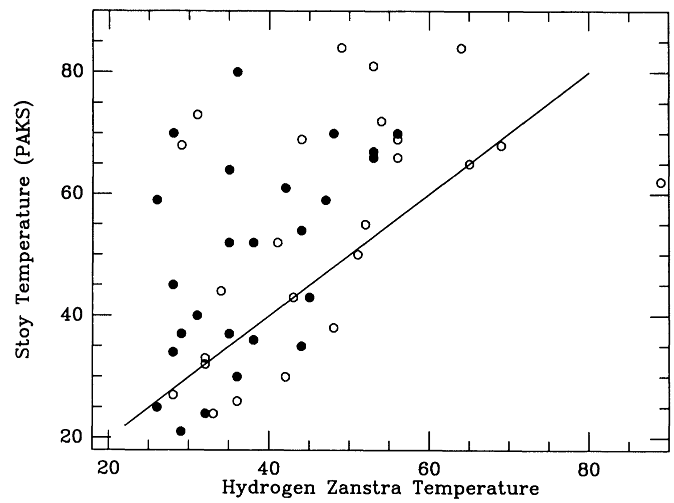

FIG. 15.—T_{PAKS} plotted against T_Z(H). The filled symbols represent the most reliable values of Zanstra temperature (asterisked in Table 1). The solid line represents perfect agreement.

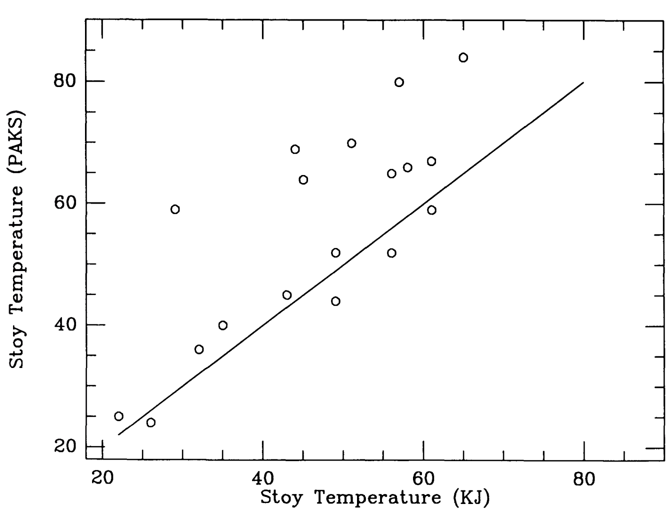

FIG. 13.—T_{PAKS} (from Preite-Martinez et al. 1989, 1990) plotted against T_S from Table 1. The solid line represents perfect agreement.

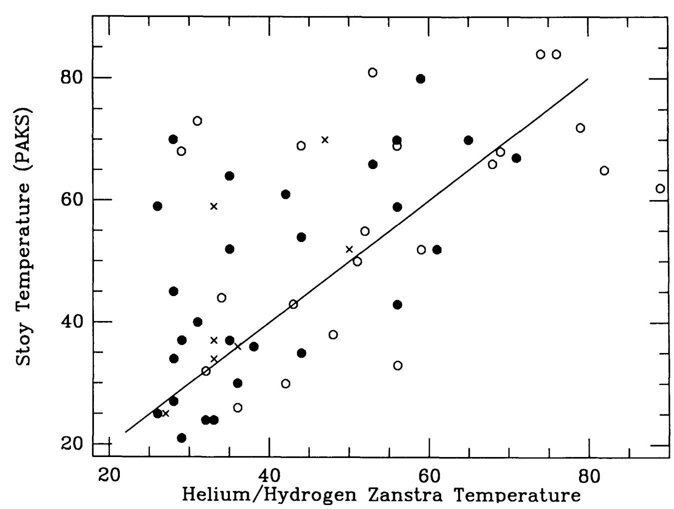

FIG. 16.—T_{PAKS} plotted against T_Z (*circles*) and T_M (*crosses*), where the filled symbols represent the most reliable Zanstra temperatures. The solid line represents perfect agreement.

with these, their lower temperature objects show reasonably good agreement, consistent with Figure 13.

We conclude that since the T_S in Table 1 show so much better general agreement with T_Z (compare with Figs. 7–10) that they are the ones to be used. The technique used to derive T_{PAKS}, though it places most of the stars in the lower temperature region (below about 70,000 K), tends strongly to overestimate temperatures and does not give sufficiently accurate values to be useful.

4. INTERPRETATION

Our goal here is to find the most self-consistent agreement among the various ways of determining the central star temperatures so as to be able to use the [O III] λ5007 line reliably in their statistical estimations and perhaps also to be able to make some progress in understanding the origin of the Zanstra discrepancy. First assume that only optical depth effects are invvolved. Like the Zanstra temperatures, the Stoy temperatures are also affected by optical depth and will also be lower limits for optically thin nebulae. However, since the Stoy method involves the division of the heating rate by the cooling rate and ignores the central star itself (see Kaler 1976a), the resulting temperature is not so sensitive to optical depth as is the Zanstra method, and we would expect T_S to be higher than T_Z(H) and to fit better with T_Z(He II). Alternatively, there may be an excess of ionizing radiation at the He^+ Lyman limit; if the nebulae were optically thick, then T_S would equal T_Z(H), and T_Z(He II) would be greater than both T_Z(H) and T_S. We might also quite reasonably have a combination of the two effects. What now do the temperature comparisons tell us?

First, notice the similarity between the distributions of points in Figures 1, 4, and 5. Even though the dispersions in Figures 4 and 5 are much the greater, the slopes are almost identical; this similarity can be seen simply by examining equations (1), (5), and (6). That is, we obtain similar temperatures from I(λ5007) by assuming the Stoy calibration and by using that found by combining T_Z(H) and T_Z(He II) into T_Z. The agreement is actually somewhat better between Figures 1 and 4, even though the error is smaller for the restricted set than it is for the full set. The close agreement among these figures suggests that the errors in the magnitudes are largely random in nature.

The agreement between the Stoy calibration and that for T_Z(H) (Figs. 1, 2, and 3; eqs. [1], [3], and [4]) is markedly poorer than it is for T_Z. The Stoy temperatures do not fit as well with the T_Z(H), and rise notably faster with increasing I(λ5007), suggesting that the nebulae start off as optically thick and tend to become optically thin—leading to low T_Z(H)—as temperature climbs significantly above about 40,000 K and He^+ ionization approaches, whereupon we should substitute T_Z(He II) for T_Z(H). The agreement is worse with the presumably more reliable restricted set than it is with the full set, suggesting here that there may in fact be some systematic magnitude effects. These comparisons imply that optical depth effects are important and can explain the Zanstra discrepancy.

However, the direct comparison among the temperatures in Figures 7, 8, 9, and 10 give a somewhat different view. The best fit is now between T_S and the full set of T_Z(H); equation (9) shows that the slope is almost unity, which would demonstrate the nebulae to be optically thick even through the domain in which the He II lines appear, suggesting that there is an He^+ Lyman excess. However, the presumably more reliable restricted set (Fig. 8; eq. [10]) shows again that T_S tends to be higher than T_Z(H), the difference increasing with temperature, much as we saw from the comparisons with I(λ5007), returning us again to the optical depth effects (supported by the fact that the slope in Fig. 10, eq. [12], is still fairly close to unity). The direction in the change between Figures 2 and 3 and between Figures 7 and 8 is the same, it is just that Figures 1 and 2 both show a slope difference, whereas Figure 7 shows a slope of unity. The errors are about the same for both sets and provide no guidance. The direct comparisons among temperatures are bound up with statistical problems involving individual errors. In addition, the number of objects is reduced since the stars must have *both* Zanstra and Stoy determinations. Part of the reason for the different possible conclusions lies in the large scatter in the λ5007 comparisons in Figures 2 through 5. Two nebulae with high I(λ5007), for example, can have quite different Zanstra temperatures. But when we compare the temperatures directly with one another, much of the scatter goes away, suggesting that this might indeed be the best approach. The question is: which is better for comparison between T_S and T_Z(H), the full set or the restricted set?

Figure 11 might provide some guidance, as it is consistent with the expected optical depth effect. The T_S tend to agree with T_Z(He II) at the lowest temperatures and then drop below as temperature increases, and are intermediate between T_Z(H) and T_Z(He II). The optical depth argument is marginally supported by Figure 12, in which T_Z(H) fits better with T_M for low temperature but falls well below it above 40,000 K, suggesting that the nebulae may be becoming optically thin. This is quite a weak argument as it is based on only two "thin" points. The nebular model results (the footnoted T_M values in Table 1), however, tend (again quite marginally) to support this contention. Below 50,000 K all the T_M are from Méndez et al., whereas all the model results range from 50,000 K and up (we ignore the Méndez et al. points *at* 50,000 K). Below 50,000 K T_M/T_S and T_M/T_Z(H) are similar and equal 1.12 and 1.17 respectively, whereas from 50,000 K and above they respectively equal 1.09 and 1.29; that is, the T_Z(H) at high temperature are somewhat too low. The difference is just barely statistically significant. Moreover, the three T_M/T_Z(He II) average 1.05. These ratios are all consistent with the nebulae becoming marginally thin somewhere around 50,000 K.

Further support comes from by just looking at some nebular morphologies: NGC 6543, NGC 6826, NGC 6891, and IC 4593 all have large outer structures (Kaler 1974), as do NGC 6369 (Jewitt, Danielson, & Kupferman 1986; Chu, Jacoby, & Arendt 1987) and IC 3568 (Chu et al. 1987), showing that, for at least some of the lower excitation nebulae, radiation is leaking out of the main object. The Stoy temperatures of the central stars of these obviously thin objects range from 43,000 to 65,000 K and all have T_Z(H) less than or equal to T_S, four of them substantially so, as expected for optically thin nebulae [one of them, NGC 6891, also has $T_Z(\mathrm{H}) \ll T_M$]. This range in temperature is consistent with the distribution of points in Figure 11. The argument is somewhat weak because of the small number of objects involved; there is as yet no evidence that the others have illuminated outer shells or halos. On the basis of its T_M and T_Z(H) we predict that IC 4637 (the other low point in Fig. 12) has a faint as-yet undetected outer shell.

Additional insight might come from Figure 17, in which we plot the Zanstra discrepancy, T_Z(He II)/T_Z(H), and the analogous ratio T_S/T_H, against I(λ5007). Here we see a reflection of the above discussions. The T_S/T_Z(H) begin at the left below unity and then show a gradual rise. With the full set the rise is

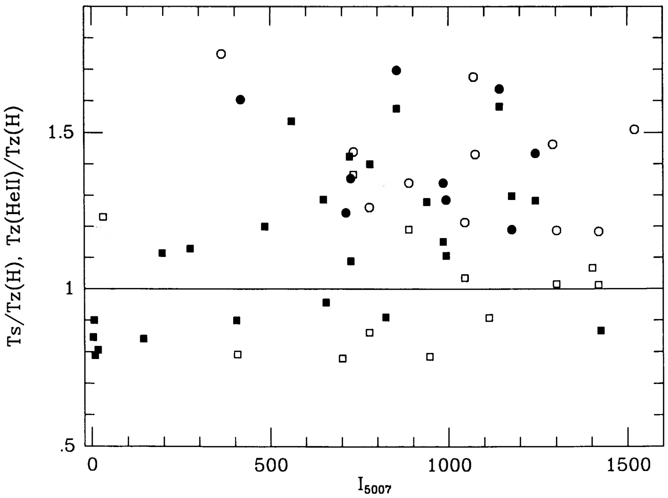

FIG. 17.—The Zanstra discrepancy, T_Z(He II)/T_Z(H) (*circles*), and the ratio T_S/T_Z(H) (*boxes*), plotted against $I(\lambda5007)$. The filled symbols denote members of the restricted (best data) set.

not so evident, but with the restricted set we see that there is evidence that the nebulae become optically thin very roughly above a λ5007 strength of 500 or so, corresponding to a temperature of near 40,000 K (note and compare Figs. 1, 2, 3, 7, and 8). However, the Zanstra discrepancies in Figure 17 show no significant correlation with $I(\lambda5007)$, but rather a flat distribution with a mean value of 1.4 and a median of 1.35. That is, when the He II lines begin to turn on at roughly 50,000 K, the Zanstra discrepancy appears already to be well in place (as demonstrated in Fig. 11 as well). This effect is consistent with the nebulae becoming optically thin well before the onset of the He II lines.

However, this graph has some similarity with the theoretical plot from Henry & Shipman (1986), in which they show that for hydrogen atmospheres the Zanstra discrepancy starts out high at 40,000 to 50,000 K and then diminishes as effective temperature increases. That is, the stars do not behave like blackbodies but have sharp emission edges, supporting the conclusions of Méndez et al. (1988). Unfortunately, the number of objects with reliable weak He II line measurements is small, so that the conclusions must remain ambiguous. Even if these edges exist for objects like these they apparently disappear when the stars become very hot (Kaler & Jacoby 1989; Jacoby & Kaler 1989), as also suggested by the work of Henry & Shipman (1986).

Two further points should be considered here. First, although the T_S have been a base in this paper against which the Zanstra temperatures have been compared, they have not been independently tested and could well contain systematic errors [suggested by the fact that the T_S may be generally lower than T_Z(H) and are lower than T_M at low temperatures]. Second, we implicitly assume that nebular evolution and optical depth monotonically follow stellar evolution. In fact, the relation depends on nebular masses, stellar masses and evolutionary rates, and expansion velocities, considerably jumbling the correlation between optical depth and central star temperature, and quite likely contributing to the scatter in the correlations between T_S, T_Z(H), and T_Z(He II).

In summary, we feel the evidence suggests that the correlation with temperatures found from Kaler's (1976a, 1978a) application of the Stoy method and $I(\lambda5007)$ (eq. [2]) is the best to use. Comparison among all the temperatures is not unambiguously clear as regards the optical depths of the nebulae. Most evidence suggests that the differences are due at least in part to the nebulae becoming optically thin somewhere in the 40,000 K–50,000 K range, such that the Zanstra discrepancy is in place at the onset of the He II lines, a value lower than has previously been assumed. However, that conclusion rests to a degree upon our (not unreasonable) adoption of the restricted—best data—set of T_Z(H). Adoption of all the data and the agreement between theory and observation of the size of the Zanstra discrepancy at the onset of He II suggest that there may well be an ultraviolet excess to consider among this set of stars. Both effects may be at work.

These results are compromised by a paucity of data. New and improved magnitudes of central stars are badly needed to improve the Zanstra temperatures, especially for the objects not marked with asterisks in Table 1. We also need more accurate intensities of the weak He II lines in the higher excitation nebulae. Several of these in fact may still originate in the central star itself. Nevertheless we believe that we have made some inroads into the examination of the subject, have outlined a way of further exploration, and most significantly, have provided a reasonably good means for easily estimating the temperatures of central stars in low-excitation nebulae, one that is especially important for studying those in external galaxies.

This work was supported in part by the National Science Foundation through grant number AST 88-13686 to the University of Illinois. We are grateful to T. Isobe for providing the linear least-squares computer program.

REFERENCES

Acker, A., Köppen, J., Stenholm, B., & Jasniewicz, G. 1989, A&AS, 80, 201
Aller, L. H., & Czyzak, S. J. 1976, private communication
Aller, L. H., & Keyes, C. D. 1987, ApJS, 65, 405
Ambartsumyan, V. A. 1932, Pulkovo Obs. Circ., 8, No. 4
Barker, T. 1978, ApJ, 219, 914
Cahn, J. H., Kaler, J. B., & Stanghellini, L. 1990, in preparation
Capriotti, E. R., & Daub, C. T. 1960, ApJ, 132, 677
Chu, Y.-H., Jacoby, G. H., & Arendt, R. 1987, ApJS, 64, 529
Collins, G. W., Daub, C. T., & O'Dell, C. R. 1961, ApJ, 133, 471
de Freitas-Pacheco, J. A., Codina, S. J., & Viadana, L. 1986, MNRAS, 220, 107
Gathier, R., & Pottasch, S. R. 1988, A&A, 197, 266
Harman, R. J., & Seaton, M. J. 1964, ApJ, 140, 824
Harrington, J. P., & Feibelman, W. A. 1983, ApJ, 265, 258
Heap, S. R., & Hintzen, P. M. 1990, ApJ, 353, 200
Henry, R. B. C., & Shipman, H. L. 1986, ApJ, 311, 774
Isobe, T., Feigelson, E. D., Akritas, M. G., & Babu, G. J. 1990, AJ, submitted.
Jacoby, G. H. 1988, ApJ, 333, 193
Jacoby, G. H., & Kaler, J. B. 1989, AJ, 98, 1662
Jewitt, D. C., Danielson, G. E., & Kupferman, P. N. 1986, ApJ, 302, 727
Kaler, J. B. 1974, AJ, 79, 594
———. 1976a, ApJ, 210, 843
———. 1976b, ApJS, 31, 517
———. 1978a, ApJ, 220, 887
———. 1978b, ApJ, 226, 947
———. 1980, ApJ, 239, 78
———. 1983a, ApJ, 264, 594
———. 1983b, ApJ, 271, 188
———. 1989, in IAU Symposium 131, Planetary Nebulae, ed. S. Torres-Peimbert (Dordrecht: Kluwer), 229
Kaler, J. B., & Jacoby, G. H. 1989, ApJ, 345, 871
———. 1990, ApJ, in press
Kohoutek, L., & Martin, W. 1981a, A&A, 94, 365
———. 1981b, AAS, 44, 325
Martin, W. 1981, A&A, 98, 328

Méndez, R. H., Kudritzki, R. P., & Simon, K. P. 1985, A&A, 142, 289
Méndez, R. H., Kudritzki, R. P., Herrera, A., Husfeld, D., & Groth, H. G. 1988, A&A, 190, 113
Natta, A., Pottasch, S. R., & Preite-Martinez, A. 1980, A&A, 84, 284
O'Dell, C. R. 1962, ApJ, 135, 371
———. 1963, ApJ, 138, 293
Pottasch, S. R., Wesselius, P. R., Wu, C.-C., Fieten, H., & van Duinen, R. J. 1978, A&A, 62, 95
Preite-Martinez, A., Acker, A., Köppen, J., & Stenholm, B. 1989, A&AS, 81, 309
———. 1990, A&AS, in press
Shaw, R. A., & Kaler, J. B. 1985, ApJ, 295, 537
———. 1989, ApJS, 69, 495
Stoy, R. H. 1933, MNRAS, 93, 588
Torres-Peimbert, S., & Peimbert, M. 1978, Rev. Mexicana Astr. Af., 2, 181
Tylenda, R., Acker, A., Gleizes, F., & Stenholm, B. 1990, A&AJ, in press
Walton, N. A., Reay, N. K., Pottasch, S. R., & Atherton, P. D. 1986, in Proc. Joint NASA/ESA/SRC Conf., New Insights in Astrophysics (ESA SP-263), 497
Webster, B. L. 1976, MNRAS, 174, 513
———. 1983, PASP, 95, 610
Zanstra, H. 1927, ApJ, 65, 50